Strongly pulsating lasers with delay

Didier Pieroux and Thomas Erneux
Université Libre de Bruxelles, Optique Nonlinéaire Théorique, Campus Plaine, Code Postal 231, 1050 Bruxelles, Belgium
(Received 5 June 1995)

A simple model of a class-*B* laser subject to a delayed feedback is investigated. The response of the laser exhibits strongly pulsating intensity oscillations which we analyze using asymptotic methods. We concentrate on a single branch of periodic solutions and progressively increase the amplitude of the feedback. We show that the response of the laser (amplitude of the oscillations and period) follows simple scaling laws which are typical to class-*B* lasers subject to optoelectronic feedback. Specifically, the intensity of the laser field quickly saturates at a constant amplitude and collapses as the feedback surpasses a critical amplitude.

PACS number(s): 42.65.Sf, 42.60.Mi

I. INTRODUCTION

Strongly pulsating intensity oscillations are commonly observed at the output of periodically modulated class-*B* lasers [1–3], and have been studied numerically [4–7] and analytically [8]. However, strongly pulsating oscillations resulting from a delayed feedback have been less investigated theoretically. The delayed feedback is an important source of numerical difficulties when the oscillations consist of sequence of spikes separated by a long period of almost constant amplitude. The lack of long-time accuracy is often ignored in numerical integration of laser delay-differential equations, and is known to lead to spurious solutions. In a series of papers, Loiko and Samson [9] and Grigorieva and Kashchenko [10] considered a variety of class-*B* lasers controlled by optoelectronic feedback and exhibiting pulsating oscillations. They proposed to describe these oscillations by approximate maps which are derived from the original laser equations. Their method consists of determining successive approximations for the passive and active parts of the oscillations which are then connected at specific times. However, their theory is not based on an asymptotic argument. In this paper, we develop an asymptotic theory for strongly pulsating oscillations. Separate approximations for the slow and fast parts of the solutions are obtained in terms of a large parameter which measures the size of the laser oscillations. The approximate solutions are compared to the numerical solution of the original laser equations. A systematic comparison between approximate and numerical solutions for different values of the amplitude parameter is missing in earlier studies [9,10], but is essential for an understanding of the validity of the map as an alternative to numerical integration.

Our approximations lead to simple expressions of the amplitude and the period of the oscillations which clarify poorly understood facts on the bifurcation diagram of lasers subject to delay. In particular, we show that the amplitude of the oscillations quickly saturates at a constant amplitude as the amplitude of the feedback is increased from zero. However, these oscillations collapse at a higher amplitude of the feedback. Our results substantiate analytically the numerical study by Otsuka and Chern [11] on a two-variable model of a laser subject to feedback. In [12], we analyzed the period-doubling bifurcation. In this paper, we concentrate on a periodic branch of solutions for different orders of magnitude of the feedback rate.

Our analysis takes advantage of the nearly conservative properties of the laser equations, which suggests introducing an energy function. As we shall demonstrate, this energy function considerably facilitates the analysis of the pulsating periodic solutions as the bifurcation parameter is progressively changed. To our knowledge, an explicit use of an energy function has never been applied to class-*B* lasers with delay, but this could be a useful tool for other more complicated laser problems such as periodically modulated lasers controlled by continuous delayed feedback [13].

The plan of the paper is as follows. The model is formulated in Sec. II. Sections III and IV concentrate on the case of small and moderate delays, respectively. Our results are discussed in Sec. V in terms of the interaction of real and delayed intensity pulses.

II. FORMULATION

A simple model of a laser with feedback was studied by Otsuka and Chern [11]. They found numerically a rich variety of bifurcation diagrams exhibiting coexisting harmonic and pulsating periodic solutions and period-doubling bifurcations [14]. In terms of dimensionless variables and parameters, the problem studied in [11] is equivalent to one of the models considered in [10], and consists of two nonlinear differential equations for the inversion of population x and the intensity of the laser field y [12]:

$$\frac{dx}{d\tau} = -y - \gamma y(\tau-\theta) - \beta x\{w + s[y + \gamma y(\tau-\theta)]\}, \quad (1)$$

$$\frac{dy}{d\tau} = x(1+y). \quad (2)$$

The variables x and y are defined as deviations from the nonzero steady state of the original laser equations. The parameters γ and θ denote the amplitude and the delay of the laser field, respectively. $w>1$ is the pump parameter normalized by its threshold value. s and β are defined by

$$s = \frac{w-1}{\gamma+1} \text{ and } \beta = K^{-1/2}s^{-1/2}, \quad (3)$$

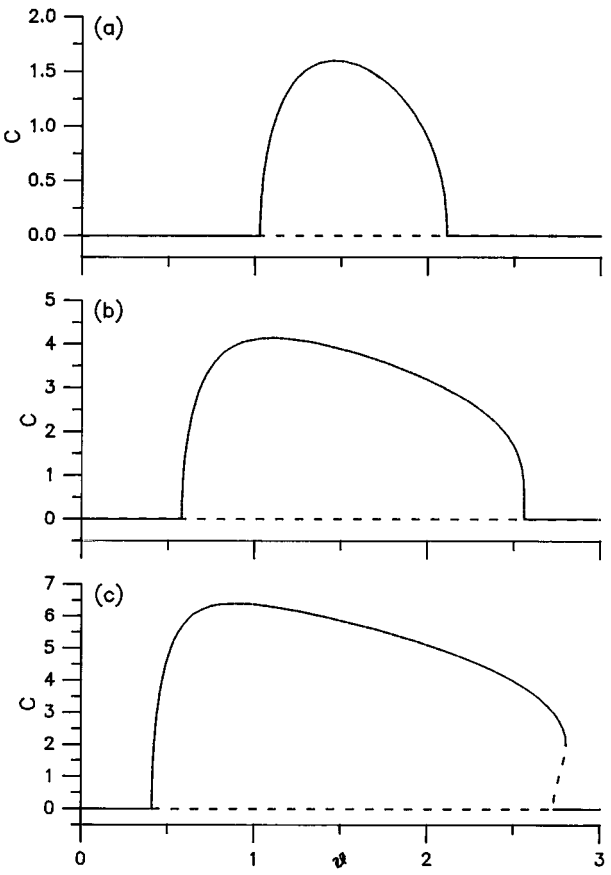

FIG. 1. Bifurcation diagrams of the first branch of the periodic solutions. The figure represents $C=\max(x)$ as a function of the delay θ. The values of the fixed parameters are $w=1.1$ and $\beta w=6\times10^{-4}$. The value of γ for each figure is (a) $\gamma=7\times10^{-4}$, (b) $\gamma=\gamma_{\text{crit}}=1.0937\times10^{-3}$, and (c) $\gamma=1.5\times10^{-3}$. Note that the direction of bifurcation changes at the second Hopf bifurcation point as $\gamma=\gamma_{\text{crit}}$. Full and dotted lines correspond to stable and unstable solutions, respectively.

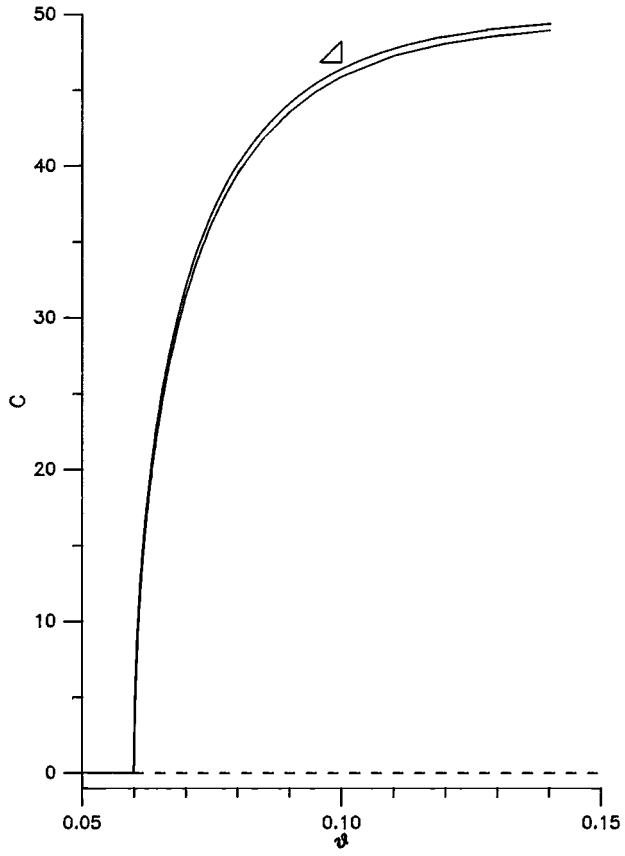

FIG. 2. Numerical and approximate bifurcation diagrams for small values of θ. The figure represents $C=\max(x)$ as a function of θ. The asymptotic approximation (indicated by an arrow) is valid for $\beta\ll\gamma\ll1$. The approximate result is given by $\max(x)=C$, where C satisfies Eq. (25). The values of the parameters are $\gamma=0.01$ and $\beta w/\gamma=0.06$.

where $K\equiv\tau_s/\tau_p$, γ_s and τ_p denote the population and the photon lifetimes, respectively. K is typically an $O(10^3$–$10^5)$ large parameter which implies that β is small. Equations (1) and (2) are physically valid, provided that the amplitude of the feedback is sufficiently small. Specifically, we shall assume that

$$\beta\ll\gamma\ll1, \tag{4}$$

and investigate the bifurcation diagram of the periodic solutions using θ as our control parameter. Large-amplitude oscillations are typically observed if inequalities (4) are satisfied. Our bifurcation analysis is guided by the linear stability analysis of the basic solution $x=y=0$ [12]. Hopf bifurcation points are located at $\theta=\theta_H$, where θ_H satisfies

$$\sin(\theta_H)=\frac{\beta w}{\gamma} \text{ and } \gamma>\gamma_c\equiv\beta w. \tag{5}$$

(If $\gamma<\gamma_c$, the basic solution is always stable). In Fig. 1, we show the first branch of periodic solutions for different values of $\gamma>\gamma_c$. The maximum of x has been computed from the averaged energy $\langle E\rangle\equiv P^{-1}\int_0^P E(\tau)d\tau$, where the function E is defined by (10) below, and P denotes the period. We then use the relation $\max(x)=C=\sqrt{2\langle E\rangle}$. In this way, we obtain an accurate value for the maximum of x which can be compared directly to our asymptotic approximation which uses the energy (10) as a starting point. Note the change of direction at the second Hopf bifurcation point in Fig. 1(c). In the following sections, we continuously increase γ and analyze how the amplitude of the solution is increasing. Because the bifurcating solution changes considerably between the two Hopf bifurcations, we need separate studies for different parts of the bifurcation diagram.

III. LOW DELAY

Figure 2 shows the bifurcation diagram for low values of θ (the figure also shows an approximation of the bifurcation diagram which is described below). It exhibits a quasivertical Hopf bifurcation, and the amplitude saturates near a constant value. We explain each modification of the solution by distinct asymptotic approximations. Each approximation reveals essential features of the solution which we emphasize. All mathematical details are deferred to the Appendix.

A. Hopf bifurcation

As θ progressively increases from zero, the basic steady-state solution changes stability at a Hopf bifurcation point $\theta=\theta_H$ which satisfies Eq. (5). Because $\beta w/\gamma$ is numerically small, θ_H can be approximated as

$$\theta_H \simeq \theta_0 \equiv \frac{\beta w}{\gamma}. \tag{6}$$

In the vicinity of $\theta=\theta_H$, the periodic solution is nearly harmonic in time, and can be constructed using a perturbation analysis. We use the fact that $\theta_H \simeq \theta_0$ is small, and simplify the expression for the amplitude derived in [12]. We find that the maximum of x is given by

$$\max(x) = 2\,\theta_0^{-3/2}[6(\theta-\theta_H)]^{1/2}. \tag{7}$$

Note that the coefficient multiplying the square root is large since θ_0 is small. From (7), we learn that the amplitude changes by an $O(1)$ quantity if the deviation $\theta-\theta_H$ is $O(\theta_0^3)$ small. This explains why the Hopf bifurcation branch appears almost vertically in Fig. 2.

B. Pulsating oscillations

After the bifurcation transition, the oscillations become progressively pulsating, i.e., y remains close to -1 except during short intervals of time where y is large. We propose to construct these pulsating solutions for small values of β and γ. Setting $\beta=\gamma=0$ in Eqs. (1) and (2) leads to the following problem for $(x,y)=(X,Y)$:

$$\frac{dX}{d\tau} = -Y, \tag{8}$$

$$\frac{dY}{d\tau} = X(1+Y). \tag{9}$$

This problem is conservative, and admits a one-parameter family of periodic solutions [12]. Its first integral motivates introducing an energy $E=E(x,y)$ defined by

$$E \equiv \tfrac{1}{2}x^2 + y - \ln(1+y). \tag{10}$$

Differentiating (10) and using Eqs. (1) and (2) leads to the following differential equation for E:

$$\frac{dE}{d\tau} = -\gamma x y(\tau-\theta) - \beta x^2\{w + s[y+\gamma y(\tau-\theta)]\}. \tag{11}$$

The right-hand side of Eq. (11) depends on x and y, but is a small quantity proportional to β and γ. This means that we may replace (x,y) by (X,Y) in first approximation, and integrate this equation. Specifically, we start at $\tau=\tau_n$, with the initial conditions

$$x(\tau_n)=x_n<0, \quad y(\tau_n)=0 \tag{12}$$

and consider a complete orbit in the phase plane (x,y) which terminates when $\tau=\tau_{n+1}$ and

$$x(\tau_{n+1})=x_{n+1}<0, \quad y(\tau_{n+1})=0. \tag{13}$$

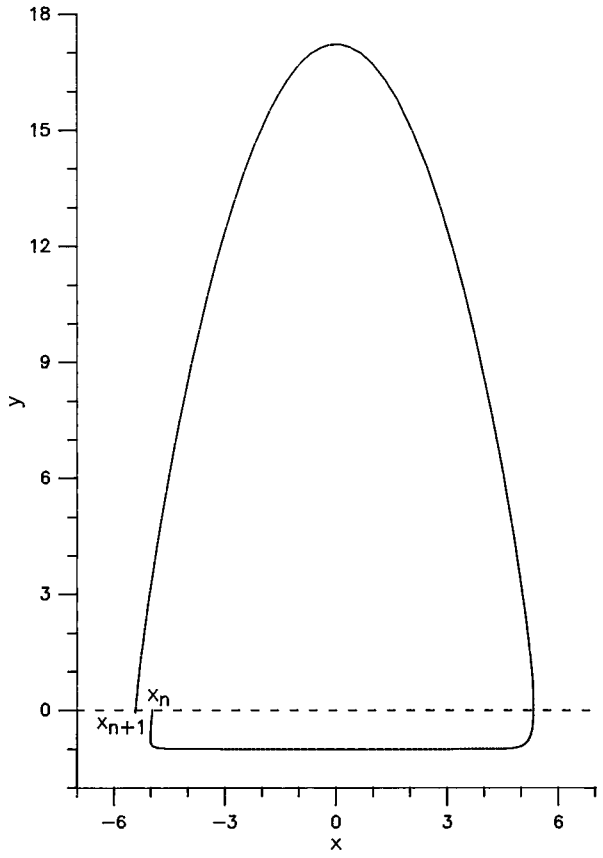

FIG. 3. Poincaré map. The change in energy is determined for a complete orbit starting at $x(\tau_n)=x_n<0$, $y(\tau_n)=0$, and finishing at $x(\tau_{n+1})=x_{n+1}<0$, $y(\tau_{n+1})=0$. The values of the parameters used in the figure are $\gamma=0.05$, $\beta w/\gamma=0.06$, and $x_n=-4.97$.

See Fig. 3. Using (10), we may then compute the initial and final energies, i.e., $E_n \equiv \frac{1}{2}x_n^2$ and $E_{n+1} \equiv \frac{1}{2}x_{n+1}^2$. We wish to find equations for the change $E_{n+1}-E_n$ and the period $\tau_{n+1}-\tau_n$. From Eq. (1) and using (8), the equation for the period is

$$\tau_{n+1}-\tau_n = -\int_{x_n}^{x_{n+1}} \frac{dX}{Y} + O(\beta,\gamma), \tag{14}$$

where $Y=Y(X)$ satisfies Eq. (10), with $E=E_n$, $x=X$, and $y=Y$. Integrating Eq. (11) from $\tau=\tau_n$ to $\tau=\tau_{n+1}$, we then obtain an equation for the energy,

$$E_{n+1}-E_n = -\gamma\int_{\tau_n}^{\tau_{n+1}} XY(t-\theta)\,dt - \beta w\int_{\tau_n}^{\tau_{n+1}} X^2\,dt + O(\beta^2,\beta\gamma,\gamma^2), \tag{15}$$

where we have used the fact that the integral of X^2Y for a closed orbit is zero.

Equations (14) and (15) are the result of an asymptotic analysis based on small values of β and γ. We now evaluate the integrals in these equations. To this end, we use an approximation for X and Y which is valid for large-amplitude pulsating solutions. The approximation is obtained from (8) and (9) by using the method of matched asymptotic expansions [15], and the leading uniform solutions is given by [16]

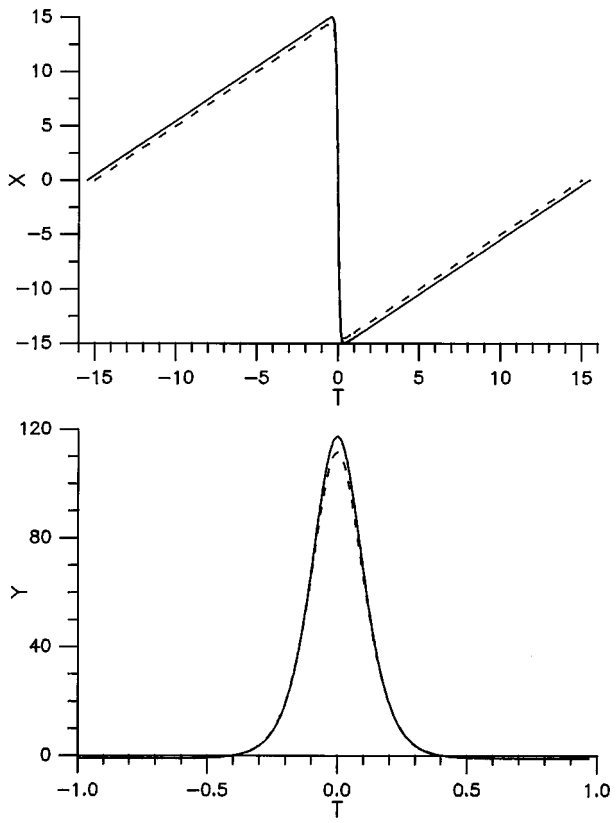

FIG. 4. Periodic solution of the leading conservative problem (8) and (9) (full line). An approximation of the solution valid for large amplitude (large C) is given by (16) and (17). They are shown by dotted lines ($C=15$).

$$X \simeq T + C\left[\frac{1-\exp(CT)}{1+\exp(CT)}\right], \tag{16}$$

$$Y \simeq 2C^2\left[\frac{\exp(CT)}{[1+\exp(CT)]^2}\right], \tag{17}$$

where $C \gg 1$ is a large parameter measuring the amplitude of the solution, and T is another time variable. C and T are defined by

$$C \equiv -x_n. \tag{18}$$

$$T \equiv \tau - \tau_n - C. \tag{19}$$

Functions (16) and (17) are defined for the interval $-C \leqslant T \leqslant C$, and are compared to the exact numerical solution in Fig. 4. The period and the maximum of x are given by

$$\tau_{n+1} - \tau_n \simeq 2C, \tag{20}$$

$$\max(x) \simeq C. \tag{21}$$

The evaluation of the integrals in the energy equation (15) depends on θ. We analyze each case in Sec. III C.

C. Poincaré map and fixed points

We first consider a small delay defined by the scaling

$$\theta = O(C^{-1}). \tag{22}$$

In this case, the intensity pulses $y(\tau)$ and $y(\tau-\theta)$ are clearly overlapping. We determine the integrals in (15). All details are given in the Appendix. We obtain the following result:

$$E_{n+1} - E_n = -2\gamma C^2 f(\psi) - \tfrac{2}{3}\beta w C^3, \tag{23}$$

where $\psi \equiv C\theta$, and $f(\psi)$ is defined by

$$f(\psi) \equiv \frac{1+\exp(\psi)}{1-\exp(\psi)} + \frac{2\psi\exp(\psi)}{[1-\exp(\psi)]^2}. \tag{24}$$

Finally, we may express C in terms of the energy E_n since $C=(2E_n)^{1/2}$. Equation (23) is a one-dimensional map for the change of energy (or amplitude) after each complete orbit in the phase plane (x,y). Knowing the energy E_n (or C) then gives the period and the amplitude of the solution using (20) and (21).

Periodic solutions of the original laser equations correspond to fixed points of the map. With $E_{n+1}=E_n$, Eq. (23) leads to the condition

$$\gamma f(\psi) + \tfrac{1}{3}\beta w C = 0. \tag{25}$$

In Fig. 2, we have represented $C \simeq \max(x)$. Using Eq. (23), we have found that this solution is always stable. The limits $\psi \to 0$ (equivalently, $\theta \to 0$) and $\psi \to \infty$ (equivalently, $\theta \to \infty$) are instructive. From (25), we find

$$\theta \to \theta_0 \ll 1 \quad \text{as} \quad \psi \to 0 \tag{26}$$

and

$$C \to C^* \equiv \frac{3}{\theta_0} \gg 1 \quad \text{as} \quad \psi \to \infty. \tag{27}$$

Thus the branch of periodic solutions connects the approximation of the Hopf point given by (6), and approaches a constant at $\theta \to \infty$. The behavior of the solution for $\psi = C\theta$ large (equivalently, $\theta \gg C^{-1}$) suggests that there exists a better approximation of the solution for $\theta = O(1)$. This problem is analyzed in Sec. IV.

IV. MODERATE DELAY

In Sec. III, we found that the branch of periodic solutions approaches a constant as $\psi = C\theta \to \infty$. In this section, we investigate this region by assuming

$$\theta = O(1). \tag{28}$$

Because of (28), the pulses $y(\tau)$ and $y(\tau-\theta)$ do not overlap significantly, which implies a different limit for the integrals in (15).

The numerical bifurcation diagram for the periodic solutions, and for $\theta = O(1)$, is shown in Fig. 5. The bifurcation diagram exhibits an almost vertical bifurcation near $\theta = \theta_H$, which we studied in Sec. III. We note that the branch of stable periodic solutions terminates by a limit point. In the

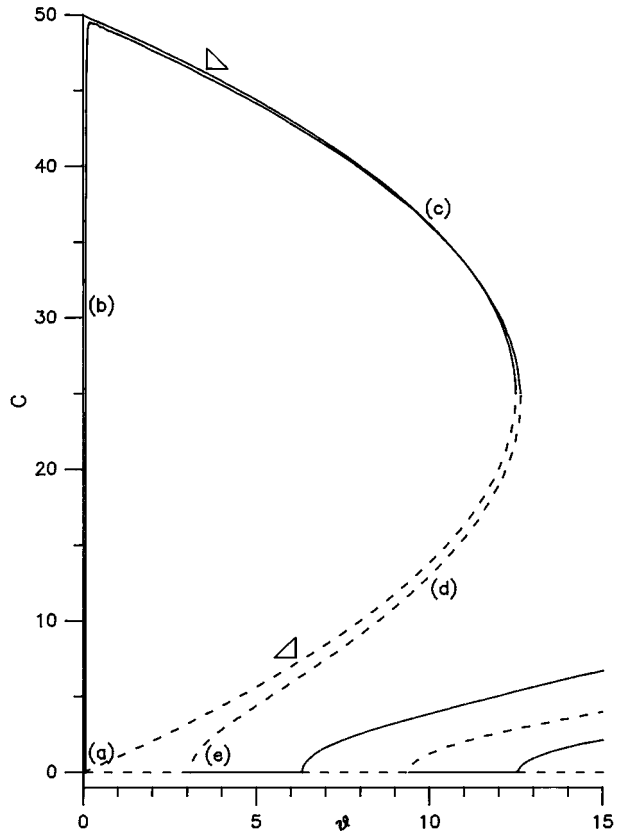

FIG. 5. Numerical and approximate bifurcation diagrams of the periodic solutions for low and moderate values of θ. The asymptotic approximation (indicated by an arrow) is valid provided that γ and β are sufficiently small. It is given by $C=\max(x)$, where C is given by (31). Stable and unstable solutions correspond to full and dotted lines, respectively. Note that the amplitude of the first branch of periodic solutions is much higher than the other branches of periodic solutions which are emerging from Hopf bifurcation points located at $\theta\simeq 2\pi$, 3π, and 4π. The oscillations are nearly harmonic for these branches, and may coexist with the first branch of pulsating periodic solutions. The solution at different points of the first branch of solutions [indicated by the labels (a)–(e)] are shown in Fig. 6. The values of the parameters are $\gamma=0.01$ and $\beta w/\gamma=0.06$.

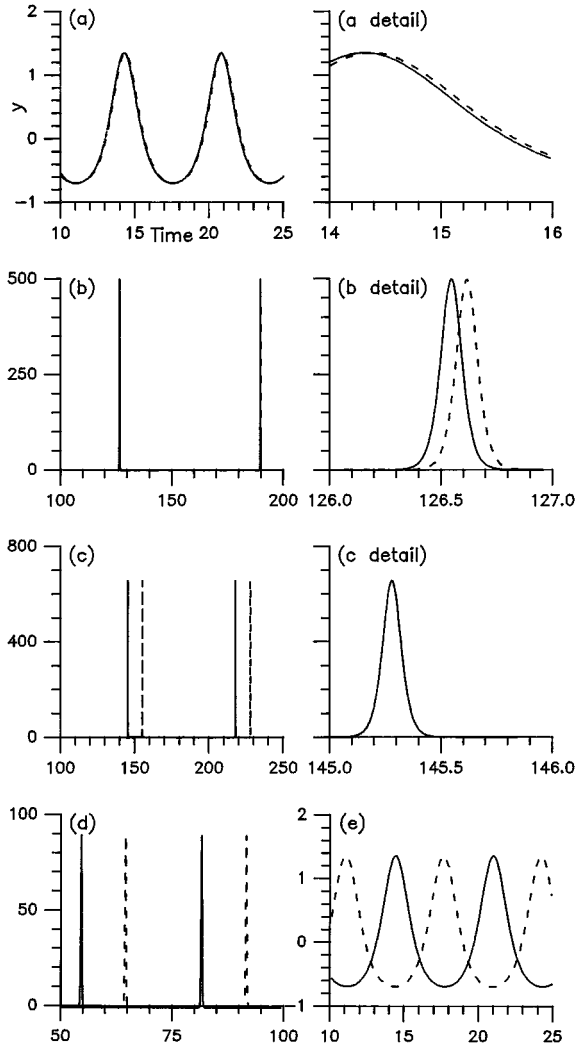

FIG. 6. Harmonic and pulsating solutions. Each figure represents $y(\tau)$ and $y(\tau-\theta)$ by full and dotted lines, respectively. The overlap between the real and delayed pulses is shown in detail on a separate figure. Each figure corresponds to a specific point indicated in Fig. 5. (a) $\theta=0.060\,044\,5$. The value of θ is slightly above the first Hopf bifurcation point located at $\theta_H=0.06$. As a result, $y(\tau)$ is nearly harmonic in time. (b) $\theta=0.07$. θ is still close to θ_H but $y(\tau)$ is already pulsating. Note that $y(\tau)$ and $y(\tau-\theta)$ are clearly overlapping. (c) $\theta=10$, upper branch. θ is now far from θ_H. $y(\tau)$ and $y(\tau-\theta)$ are spiking at different times, and no overlap between these pulses are observed. As a result, the amplitude of the solution remains almost constant as θ is varied. (d) $\theta=10$ but lower branch. The distance between $y(\tau)$ and $y(\tau-\theta)$ is close to half of the period. (e) $\theta=3.215\,91$. θ is close to the second Hopf bifurcation point. $y(\tau)$ is again harmonic but unstable, and $y(\tau-\theta)$ is π shifted.

Appendix, we reevaluate the first integral in Eq. (15) and obtain the following equation for $E_{n+1}-E_n$:

$$E_{n+1}-E_n=-2C\gamma(\theta-C)-\tfrac{2}{3}\beta wC^3 \quad (\theta<C). \tag{29}$$

From this equation, we obtain a quadratic equation for the fixed points $E_{n+1}=E_n$ given by

$$\tfrac{1}{3}\beta wC^2-\gamma C+\gamma\theta=0. \tag{30}$$

The two real and positive roots are

$$C=C_{\pm}\equiv\frac{\gamma\pm(\gamma^2-4\theta\beta w/3)^{1/2}}{2\beta w/3} \quad (\theta\leqslant\theta_L\equiv 3\gamma^2/4\beta w). \tag{31}$$

(31) corresponds to two distinct branches connected at the limit point $\theta=\theta_L$. Note the limiting behavior of C_+ and C_-:

$$C_+\to C^* \quad \text{and} \quad C_-\to\theta \quad \text{as} \quad \theta\to 0. \tag{32}$$

Thus C_+ matches our previous approximation for $\theta=O(C^{-1})$, and C_- approaches the limit $C=\theta$. A separate analysis is then necessary in order to show that this branch of solutions is connecting a second Hopf bifurcation point located at $\theta_H\simeq\pi$. Using (29), we have verified that C_+ is stable and C_- is unstable. The unstable solutions have been obtained numerically by using a continuation method.

V. DISCUSSION

We have analyzed a single branch of periodic solutions which emerges and terminates at a Hopf bifurcation. We derive a simple map for the change of energy after each oscillation. This leads to a condition for the maximum amplitude of the periodic solution. Our asymptotic analysis is successful in predicting the various changes of the amplitude as the control parameter is changed, as well as the stability of the solution. In this section, we review our main results and emphasize the different behaviors of the intensity. Of particular interest is the relative behaviors of the real and delayed intensity pulses given by $y(\tau)$ and $y(\tau-\theta)$, respectively. For low values of θ, $y(\tau)$ and $y(\tau-\theta)$ are harmonic in time and are overlapping completely; see Fig. 6(a). Slightly increasing θ leads to periodic pulsating oscillations and $y(\tau)$ and $y(\tau-\theta)$ overlap partially; see Fig. 6(b). This overlap disappears for larger values of θ, and the amplitude of the solution remains almost constant as θ is further increased; see Fig. 6(c). Finally, we note that the amplitude of $y(\tau)$ decreases smoothly as θ approaches half of the period; see Fig. 6(d). This last feature cannot be understood in terms of $y(\tau)$ and $y(\tau-\theta)$, but rather in terms of $x(\tau)$ and $y(\tau-\theta)$, which are the key variables changing the energy [see Eq. (11)]. As θ approaches half of the period, $x(\tau)$ approaches zero, which explains the decrease of the energy. Figure 6(e) shows the periodic solution near its second Hopf bifurcation point.

The idea of describing pulsating oscillations by a map for a laser subject to a delayed feedback was first proposed in [9] and [10]. The map is obtained by patching different approximations of the solution at specific times. The method works best when the real delayed intensity pulses appear at different times (i.e., weak or no overlap). However, when the intensity pulses are partially overlapping, we have found that the energy of the nearly conservative oscillations is a useful function. It is the condition for a bounded energy that leads to an integral condition which can be solved systematically for all possible cases.

ACKNOWLEDGMENTS

This research was supported by the U.S. Air Force Office of Scientific Research Grant No. AFOSR-93-1-0084, the National Science Foundation Grant No. DMS-9308009, the Fonds National de la Recherche Scientifique (Belgium), and the InterUniversity Attraction Pole of the Belgian government.

APPENDIX

1. Small $\theta = O(C^{-1})$

In this appendix, we determine the two integrals in Eq. (15) by using the approximations (16) and (17). We have

$$I_1 \equiv \int_{\tau_n}^{\tau_{n+1}} XY(t-\theta)dt = \int_{-C}^{C} XY(T-\theta)dT \tag{A1}$$

$$\simeq 2C^2 \int_{-\infty}^{\infty} \frac{1-\exp(\xi)}{1+\exp(\xi)} \frac{\exp(\xi-\psi)}{[1+\exp(\xi-\psi)]^2} d\xi \tag{A2}$$

as $C\to\infty$. $\xi \equiv CT$, and ψ is defined by

$$\psi \equiv C\theta. \tag{A3}$$

We solve the integral by substitution and partial fractions, and obtain

$$I_1 = 2C^2 f(\psi) = 2C^2 \left[\frac{1+\exp(\psi)}{1-\exp(\psi)} + \frac{2\psi\exp(\psi)}{[1-\exp(\psi)]^2} \right]. \tag{A4}$$

The second integral in Eq. (15) is given by

$$I_2 = \int_{\tau_n}^{\tau_{n+1}} X^2 dt = \int_{-C}^{C} X^2 dt \tag{A5}$$

$$\simeq \int_{-C}^{0} (C+T)^2 dt + \int_{0}^{C} (-C+T)^2 dT$$

$$= \tfrac{2}{3} C^3. \tag{A6}$$

2. Moderate $\theta = O(1) < C$

We start with I_1 given by (A1), and introduce the variable $\xi = C(T-\theta)$. Assuming $\theta < C$, we find

$$I_1 \simeq 2C^2 \int_{-C(C-\theta)}^{C(C-\theta)} (-C+\theta+C^{-1}\xi) \frac{\exp(\xi-\psi)}{[1+\exp(\xi-\psi)]^2} d\xi. \tag{A7}$$

As $C\to\infty$, (A7) becomes

$$I_1 \simeq 2C(\theta-C) \int_{-\infty}^{\infty} \frac{\exp(\xi-\psi)}{[1+\exp(\xi-\psi)]^2} d\xi = 2C(\theta-C). \tag{A8}$$

If $C-\theta$ is $O(C^{-1})$, we have reevaluated the integral and have found the same result.

[1] F. T. Arecchi, R. Meucci, G. P. Puccioni, and J. R. Tredicce, Phys. Rev. Lett. **49**, 1217 (1982).

[2] D. Dangoisse, P. Glorieux, and D. Hennequin, Phys. Rev. A **36**, 4775 (1987).

[3] C. Lepers, J. Legrand, and P. Glorieux, Phys. Rev. A **43**, 2573 (1991).

[4] I. B. Schwartz, Phys. Lett. **126A**, 411 (1988); Phys. Rev. Lett. **60**, 1359 (1988).

[5] H. G. Solari, E. Eschenazi, R. Gilmore, and J. R. Tredicce, Opt. Commun. **64**, 453 (1987).

[6] W. Lauterborn and R. Steinhoff, J. Opt. Soc. Am. B **5**, 1097 (1988).

[7] J. Sacher, D. Baums, P. Panknin, W. Elsasser, and E. O. Gobel, Phys. Rev. A **45**, 1893 (1992).

[8] I. B. Schwartz and T. Erneux, SIAM J. Appl. Math, **54**, 1083 (1994).

[9] N. A. Loiko and A. M. Samson, Opt. Commun. **93**, 66 (1992); Quantum Electron. **24**, 657 (1994).

[10] E. V. Grigorieva and S. A. Kashchenko, Opt. Commun. **102**, 183 (1993); Zh. Eksp. Teor. Fiz. **105**, 355 (1994) [Sov. Phys. JETP **79**, 197 (1994)]; Int. J. Bif. Chaos **3**, 1515 (1993).
[11] K. Otsuka and J.-L. Chern, Opt. Lett. **16**, 1759 (1991).
[12] D. Pieroux, T. Erneux, and K. Otsuka, Phys. Rev. A **50**, 1822 (1994).
[13] T. Erneux, S. Bielawski, D. Derozier, and P. Glorieux, Quantum Semiclass. Opt. **7**, 951 (1995).
[14] J.-L. Chern, K. Otsuka, and F. Ishiyama, Opt. Commun. **96**, 259 (1993). .
[15] J. Kervokian and J. D. Cole, *Perturbation Methods in Applied Mathematics*, Applied Mathematical Sciences Vol. 34 (Springer-Verlag, Berlin, 1981).
[16] T. Erneux (unpublished).